Two satellite study of substorm expansion near geosynchronous orbit

Ø. Holter, Patrick H. M. Galopeau, A. Roux, S. Perraut, A. Pedersen, A. Korth, T. Bösinger

**Annales
Geophysicae**

Two satellite study of substorm expansion near geosynchronous orbit

Ø. Holter[1, 2], P. Galopeau[2], A. Roux[2], S. Perraut[2], A. Pedersen[1], A. Korth[3], and T. Bösinger[4]

[1]Department of Physics, University of Oslo, Oslo, Norway
[2]Centre d'étude des Environnements Terrestre et Planétaires, CNRS-Université Versailles Saint-Quentin, Velizy, France
[3]Max-Planck-Institut für Aeronomie, 37191 Katlenburg-Lindau, Germany
[4] Department of Physics, University of Oulu, Oulu, Finland

Abstract. During several time intervals in 1979–1980 the satellites GEOS-2 and SCATHA were situated relatively close on the nightside of the Earth at geosynchronous distances. Several substorm events were identified during these periods. The event considered in this paper was recorded on 22 May 1979, when the satellites were separated by less than 30 min in local time around 21:00 LT. The observed 45 to 60 s delay of magnetic signatures observed at the two s/c indicates a westward expansion of $\sim$7.7°/min. At the two s/c, the magnetic signatures are, in particular for the azimuthal magnetic field components, quite different. At GEOS-2, being close to the magnetic equator, the dominant feature is a dipolarization with a weak field-aligned current signature corresponding to a symmetric current which cancels at the equator. On SCATHA, however, being close to the current sheet boundary, the azimuthal magnetic field indicates a strong field-aligned Birkeland current structure. On both s/c the first indication of an approaching substorm was an increase in the high energy ion flux followed by a reduction in the flux intensity of energetic electrons and a further tailward stretching of the magnetic field, starting $\sim$2 min before the onset of the magnetic field dipolarization. The tailward stretching, the observed variations of the magnetic field components, and the subsequent dipolarization are interpreted in terms of an azimuthally tilted field-aligned current system passing the s/c on the tailward side from east to west. The westward expansion and dipolarization observed at the two s/c are consistent with the propagation of a Rayleigh-Taylor type instability. The increased radial ion flux corresponds to the $\boldsymbol{E} \times \boldsymbol{B}$-drift due to the substorm associated electric field.

Key words. Magnetospheric physics (storms and substorms; plasma waves and instabilities; current systems)

1 Introduction

The substorm scenario originally proposed by Akasofu (1964), suggesting that substorms are initiated locally and subsequently expand globally, has been confirmed by a number of studies.

Prior to substorm onset, during the substorm growth phase, there is a tailward stretching of the magnetic field, which is maintained by an azimuthal neutral sheet tail current. During the substorm, the magnetic field reconfigures towards a more dipolar-like structure (Cummings et al., 1968; Fairfield and Ness, 1970).

Macroscopically, the neutral sheet current is due to the combined effect of the terrestrial magnetic field and an earthward directed pressure gradient. On the microscopic scale, however, the origin of the current is the magnetic curvature- and the gradient drifts of electrons and ions, respectively. The drift velocities of ions and electrons are in opposite directions and their contributions to the current are energy dependent. The main part of the current is presumably being carried by the westward drifting high energy ions. As a result of a fully developed substorm the magnetospheric magnetic field is reconfigured as a more dipolar structure. At geostationary distances, substorm onset and subsequent magnetic field reconfiguration are associated with a localized disruption of the azimuthal current. These large-scale changes in the magnetospheric current system have qualitatively been interpreted as an expanding current wedge (CW) (McPherron et al., 1973). Within the CW the disrupted current can be described as the original westward current with a superimposed equivalent eastward current (McPherron, 1972), with its counterpart in the ionosphere. The disruption of the azimuthal crossfield current is associated with the transition towards a dipolar magnetic field structure (e.g. McPherron et al., 1973; Nagai, 1987; Thomsen et al., 2001). At the CW boundary the current system is supposed to be closed by field-aligned Birkeland currents (FABCs) to the ionosphere.
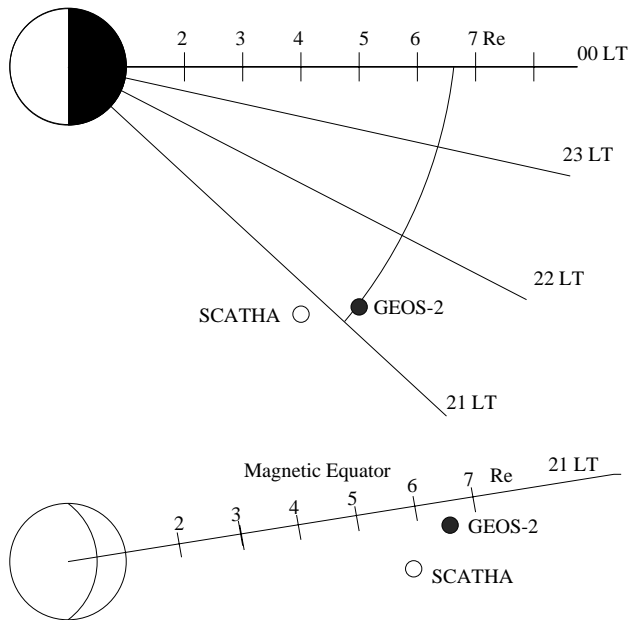
Correspondence to: Ø. Holter
(oivin.holter@fys.uio.no)

Fig. 1. Schematic illustration of GEOS-2 and SCATHA positions in the equatorial and meridian planes on 22 May 1979 at 18:40 UT.

These FABCs are indirectly observed by the appearance of azimuthal magnetic field components during substorms (Coleman and McPherron, 1976; McPherron and Barfield, 1980; Kokobun and McPherron, 1981). For symmetry reasons, the FABCs should vanish at the magnetic equator, and hence are most clearly observed some distance away from the magnetic equatorial surface (MES).

The region of disrupted current subsequently expands both azimuthally (Nagai, 1991) and radially (Jacquey et al., 1991, 1993), and ultimately, for a fully developed substorm, the entire magnetic field approaches a dipolar structure.

Substorm developments in the magnetosphere may alternatively be visualized as an expansion of a bounded dipolarized region (DPR), with a boundary (or front) separating the tailward and dipolar-like magnetic field structures, respectively. The signature of a transition from tailward to dipolar structures can be identified from the meridian magnetic field components.

A statistical study of 194 substorms recorded at geosynchronous orbit by the GOES-5 and GOES-6 satellites by Nagai (1991) indicated, on average, that substorm onsets were located in a narrow sector centered around 23:30 MLT, with subsequent expansions both west- and eastwards. The extent of the disruption region was estimated by Ohtani et al. (1991) to be of the order of, or less than, one Earth radius R_E. In a later work, Ohtani et al. (1998) found by using data from AMPTE/CCE and SCATHA, which were closely spaced in the midnight sector, that the disruption region could be of the order of the proton gyroradius.

The expansion and subsequent dipolarization of the magnetic field is associated with particle injections which are considered as independent signatures of substorm onset. The

recorded expansion of particle injection fronts exhibits more detailed structure than the corresponding magnetic dipolarization, with a time separation of electron and ion injections, depending on the local time. A two-satellite study of 43 substorm events by Thomsen et al. (2001) confirmed the azimuthal expansion of the injection region both west- and eastwards at geostationary distances.

Ohtani et al. (1992) modelled the azimuthal disrupted current vs. magnetic field and presented a method for analysing radial substorm expansions in the absence of FABCs. Using magnetic field data from the closely positioned s/c ISEE 1 and ISEE 2, a statistical study indicated onset positions for all but one event earthward of the s/c locations at 12–22 R_E. Even if the breakup location was known, one would in general need several satellites to estimate characteristic expansion properties because the DPR may have different expansion velocities in different directions as schematically illustrated by Ohtani et al. (1991).

One of the major problems in understanding substorm onset and development is the substorm trigger mechanism. Based on experimental evidence recorded at geostationary distances, Roux et al. (1991) interpreted the substorm development in terms of ballooning modes. A number of papers have addressed the ballooning instability in the near-Earth magnetosphere $<10\ R_E$ (e.g. Miura et al., 1989; Ohtani et al., 1989a,b; Ohtani and Tamao, 1993; Lee and Wolf, 1992; Lee, 1998; Hurricane et al., 1997; Bhattacharjee et al., 1998a,b; Cheng and Lui, 1998; Horton et al., 1999; Hurricane et al., 1999; Horton et al., 2001).

During several time intervals in 1979–1980 the satellites GEOS-2 and SCATHA were situated relatively close on the nightside of the Earth at geosynchronous distances. Several substorm events have been identified during these periods. In this paper we investigate a substorm which occurred on 22 May 1979, and was recorded on the two closely spaced s/c. The two s/c were separated by ∼0.65 R_E in longitude, and by ∼0.9 R_E in latitude, with GEOS-2 close to the magnetic equator and SCATHA close to the current sheet boundary. With this constellation we observe both the longitudinal rate of expansion and the latitudinal structure of the FABCs during the substorm.

In Sect. 2 we present the substorm event, and in Sect. 3 we present the data set which is used in Sect. 4 to discuss the relations between the FABCs and the time development of the magnetic field components. The possible link between the substorm and a ballooning instability is discussed in Sect. 5. Finally, Sect. 6 summarizes the discussion.

2   Substorm event: 22 May 1979

The data available from GEOS-2 and SCATHA only partially cover the same quantities, frequency ranges, and particle energy intervals. Among the accessible parameters, we have used the three components of the magnetic field with a time resolution of 5.5 s for both s/c. On GEOS-2, the two equatorial components (normal to the satellite spin

Table 1. Location of Sodankylä, and footprints of GEOS-2 and SCATHA, respectively.

		SOD	SCA	GEO
18:30 UT	E	26°38′	31°51′	37°36′
	N	67°22′	66°38′	69°00′
19:00 UT	E	26°38′	33°09′	37°36′
	N	67°22′	66°54′	69°00′

axis) of the electric field with the same time resolution of 5.5 s is available. On GEOS-2 we have high frequency 0.1 Hz$\leq f \leq$12 Hz oscillations of the magnetic field components, while on SCATHA we have recordings of the scalar electric and magnetic fields in different frequency bands in the range 0.1 Hz$\leq f \leq$ 200 Hz. Differential high energy particle fluxes of electrons and ions are available on both s/c with a time resolution of 1 min. On GEOS-2 we use the equatorial plane components of the integrated high energy ion flux intensities with a time resolution of 5.5 s. In addition, we have ground magnetogram recordings of the two horizontal magnetic field components from Sodankylä.

During the selected substorm event on 22 May 1979 at ∼18:40 UT, SCATHA and GEOS-2 were closely situated on the evening side of the Earth, as illustrated in Fig. 1 and Fig. 2. Figure 1 shows schematically the location of the two s/c in the equatorial plane and in the meridian (21:00 LT) plane, while Fig. 2 shows a more detailed perspective of the relative position of the two s/c. At 18:40 UT (21:04 LT), GEOS-2 was in a geostationary orbit at 6.6 R_E, while SCATHA was in a position 6° to the west of GEOS-2 at 20:41 LT. Further, SCATHA was 0.24 R_E radially earthward from GEOS-2, and 7.5° below the GEOS-2 orbital plane. The distance between the two s/c was 1.1 R_E.

The estimated footprints for SCATHA and GEOS-2 and the location of the Sodankylä station are summarized in Table 1. The Sodankylä station was located during the substorm to the west of the footprints of the two s/c. The onset of the dipolarization event occurred around 18:40 UT. The selected time period of 30 min begins at 18:30 UT and covers a 10 min period before the dipolarization onset and the main part of the dipolarization process as observed on the two s/c.

3 Presentation of data

Below, we present diagrams which show the time development of a number of quantities in the selected time interval. The coordinate system used for the data presentation is a satellite centered VDH system, with V radially outward, D in the azimuthal east direction, and H parallel to the spin axis of the Earth. The general trend is a clear separation into a quiet pre-substorm period ending around 18:40 UT, followed by a period characterized by a transition to a dipolar

May 22, 1979; 1840 UT
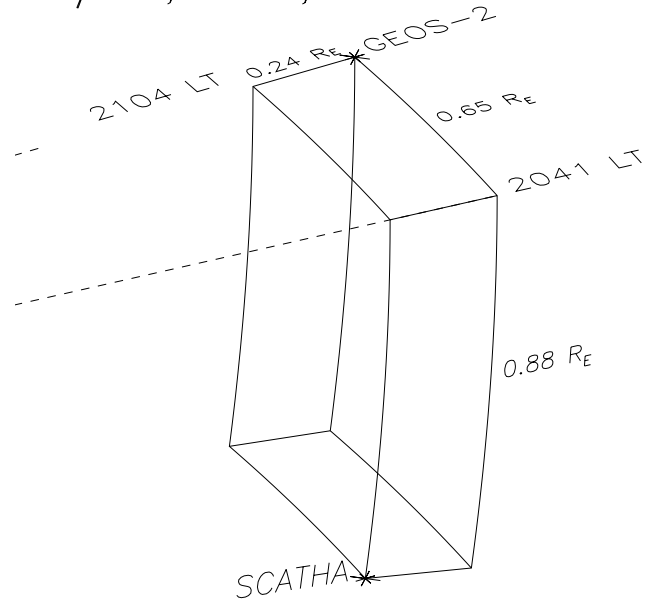
Distance SCATHA−GEOS = 1.10 R_E

Fig. 2. Relative positions of GEOS-2 and SCATHA on 22 May 1979 at 18:40 UT.

magnetic field structure accompanied by large amplitude oscillations.

3.1 Magnetic Fields

On both s/c, the recorded magnetic fields cover a wide frequency range from 0 to several Hz. The oscillations which are seen on the magnetic (and electric) field components are, to a large extent, associated with the dipolarization process. The low frequency plots exhibit the ambient magnetic field variations with superimposed low frequency oscillations.

3.1.1 GEOS-2 magnetic field

In Fig. 3 the magnetic field components recorded on GEOS-2 illustrate the combined result of a relatively slow average trend, associated with the reconfiguration of the overall magnetic field, and large amplitude irregular oscillations (Holter et al., 1995). Each magnetic component exhibits a number of minima and maxima whose identification is somewhat uncertain due to the superimposed oscillations. After ∼18:40 UT we observe on Fig. 3 large amplitude irregular oscillations on all components, and note the following characteristics:

The B_V-component decreases slowly from an initial value ∼7 nT at 18:30 UT to ∼5 nT at ∼18:40:15 UT, when it starts to increase and attains a first maximum at ∼18:41:15 UT. Subsequent large amplitude low frequency oscillations are superimposed on an average value decaying from 20 to 15 nT.
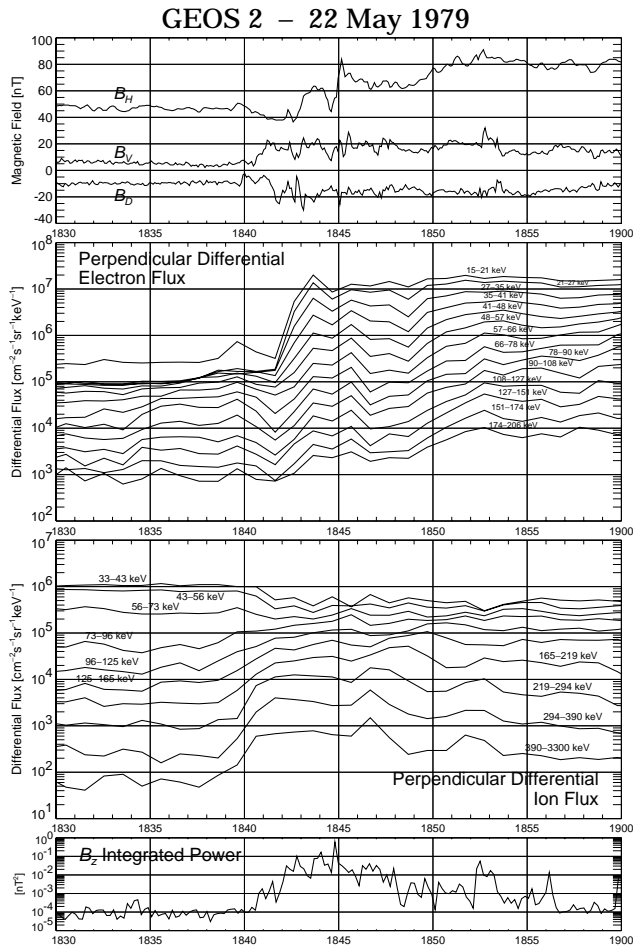
Fig. 3. GEOS-2 measurements as functions of time. From top to bottom: 1. Three magnetic field components; 2. Differential high energy electron flux intensity; 3. Differential high energy ion flux intensity; 4. Integrated power of magnetic field oscillations in frequency range 0.5–11 Hz.
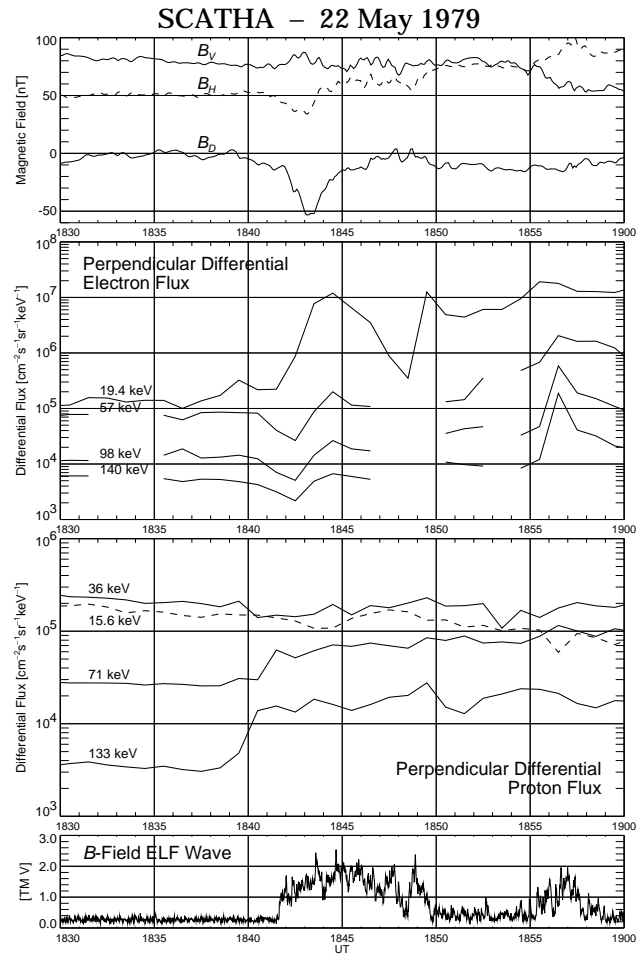

Fig. 4. SCATHA measurements as functions of time. From top to bottom: 1. Three magnetic field components, 2. Differential high energy electron flux intensity. 3. Differential high energy ion flux intensity. 4. Integrated power of magnetic field oscillations in frequency range 1.0–2.0 Hz.

The B_D-component is negative (westward) and remains almost constant around ∼10 nT until ∼18:40 UT. Following a temporary drop in magnitude, an increase accompanied by large amplitude oscillations starts at 18:41:00 UT, and a maximum level of ∼−20 nT is attained at ∼18:41:45 UT. Except for some low frequency oscillations, B_D remains, on average, almost constant at ∼−15 nT after ∼18:45 UT. A small decrease after ∼18:57 UT brings the B_D-value close to its initial value ∼−10 nT.

The B_H-component remains initially almost constant with a value ∼48 nT. At ∼18:39:45 UT it starts to decrease towards a minimum value ∼40 nT around ∼18:41:30 UT. At ∼18:42:30, B_H starts to increase rapidly in an irregular fashion, and attains an approximate maximum ∼85 nT around ∼18:52:40 UT.

3.1.2 SCATHA magnetic field

In Fig. 4 we have plotted the magnetic field components recorded on SCATHA. As on GEOS-2, we observe after ∼18:40 UT irregular oscillations on all components, however, with relative amplitudes smaller than on GEOS-2. From Fig. 4 we note the following characteristics of the three components:

The B_V-component starts at a value ∼85 nT and then decreases slowly to a value of ∼75 nT at ∼18:41:20 UT. An increase to a maximum ∼85 nT at ∼18:43:00 UT is then followed by a slowly decreasing average value around ∼77 nT. At ∼18:54:20 UT the B_V-value drops further and attains a value ∼55 nT at ∼18:57:30 UT.

The B_D-component on SCATHA starts at 18:30 UT with a value ∼−8 nT close to the value measured on GEOS-2. However, the magnitude decreases to an average around zero with superimposed low frequency oscillations. Around ∼18:39:00 UT a slow increase in magnitude commences
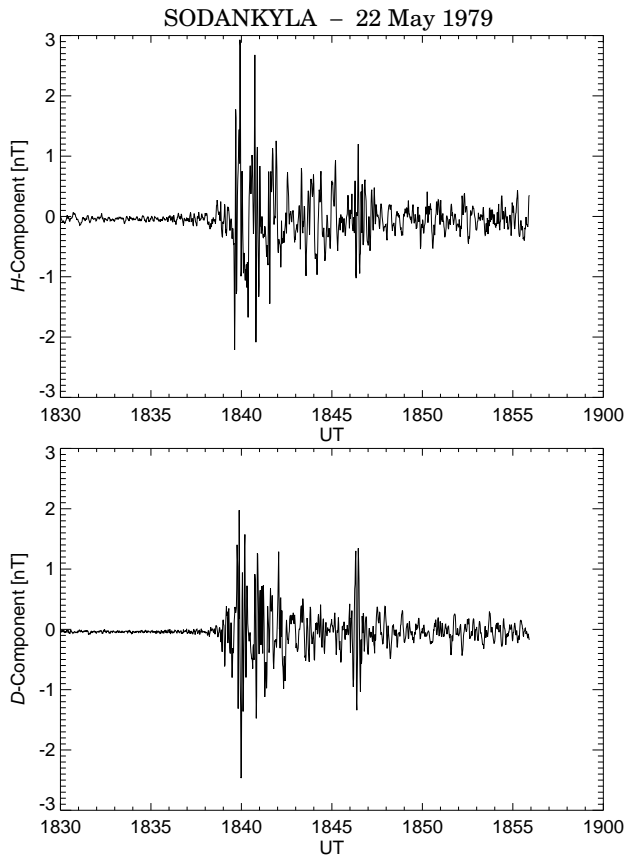
Fig. 5. Ground observations of the magnetic H- and D-components recorded at Sodankylä.

Fig. 6. Electric field V- and D-components recorded on GEOS-2 as functions of time.

followed at $\sim$18:41:40 UT by a relatively sharp increase. A maximum negative value of ~-53 nT is attained at $\sim$18:43:10 UT. Following a subsequent decrease in its magnitude, B_D attains ~-10 nT at 18:46:15 UT and a minimum magnitude close to zero at $\sim$18:47:30 UT. The magnitude of B_D then increases and remains fairly constant with slow variations around ~-10 nT for $t>18:50$ UT.

The B_H-component remains initially almost constant at a value $\sim$50 nT until $\sim$18:40:25 UT, when it starts to decrease, reaching a minimum $\sim$35 nT at $\approx$18:43:00 UT. B_H then increases and attains a maximum close to $\sim$100 nT at $\sim$18:57:10 UT.

3.1.3 Sodankylä magnetic field

In Fig. 5 we have plotted the H- and D-components of the ground magnetic field measured at Sodankylä, which is located about $11°$ to the west of the GEOS-2 magnetic footprint. On both components we observe a weak beginning of an intensification at $\sim$18:37 UT, followed by very strong intensifications beginning at $\sim$18:39 UT, and with a maximum amplitude at $\sim$18:40 UT. The oscillations persist during the whole time period, however, with amplitudes considerably below the maximum in the later part.
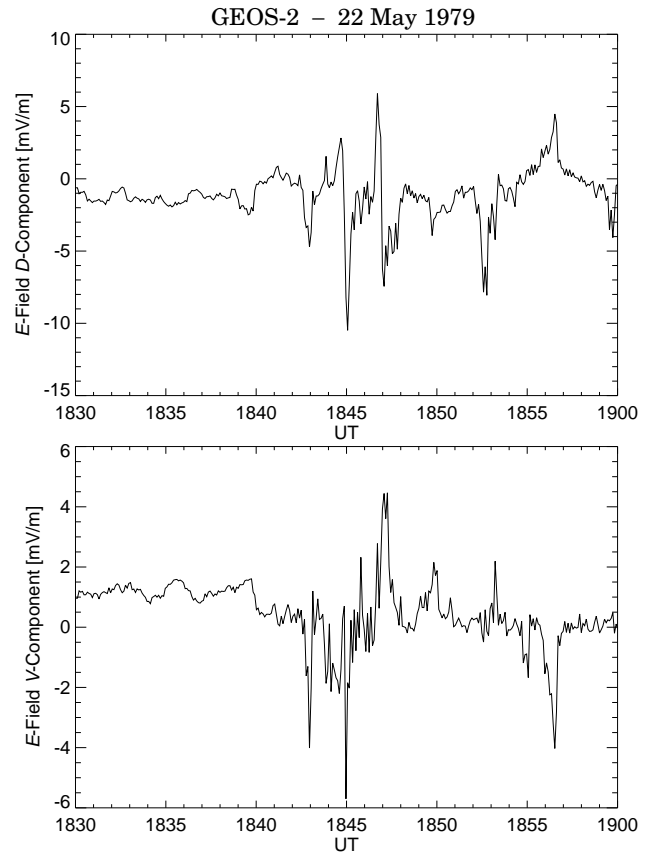
3.2 Electric field

For GEOS-2 the measured electric field components E_V and E_D are presented in Fig. 6. Before $\sim$18:40 UT, the measurements are unreliable due a bias current that is too small, and the average values appear to be constant offsets.

The E_V-component in Fig. 6 exhibits irregular oscillations around zero. The amplitudes attain values $\sim\pm4$ mV/m at 18:42:50, 18:45:00, and 18:47:00 UT.

The E_D-component in Fig. 6 clearly has an average value below zero, with irregular superimposed oscillations with maximum amplitudes $\sim\pm10$ mV/m.

3.3 High energy particle flux intensities

Both on GEOS-2 and SCATHA, measurements of high energy particle fluxes with a time resolution of 1 min are available. The measurements on GEOS-2 include both integrated and differential flux intensities and pitch angle distributions of electron and ion fluxes. The data from SCATHA covers a smaller range of parameters, but the differential high energy particle fluxes are available in energy intervals also covered by the GEOS-2 measurements.
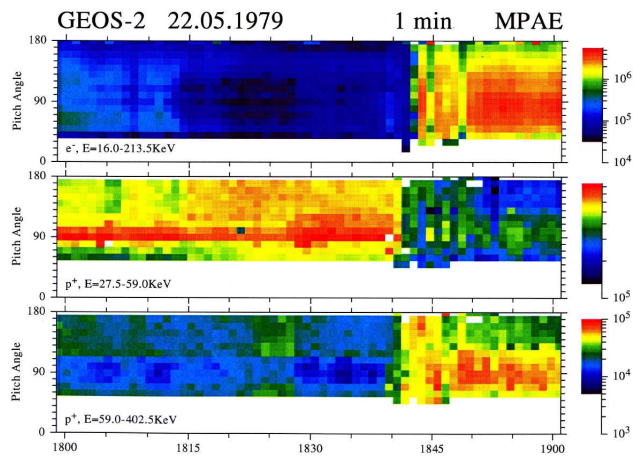
Fig. 7. Pitch angle flux intensities for high energy electrons and ions recorded on GEOS-2.

3.3.1   GEOS-2 particle flux intensities

In Fig. 3 we show for GEOS-2, the integrated differential fluxes with 1-min resolution for electrons and ions in the pitch angle range 65–115°. The energy range for electrons is from 15 to 206 keV, and for ions from 33 keV to 3.3 MeV. The energy intervals represented by the curves are indicated.

The 1-min resolution colour diagrams in Fig. 7 show the pitch angle flux intensity distribution for electrons with energies 16.0–213.5 keV, and ions for the two energy ranges 27.5–59.0 keV and 59.0–402.5 keV, respectively.

3.3.2   Electrons

The injection of electrons on GEOS-2 is seen on Fig. 3 as a simultaneous increase of the electron flux intensity on all energy channels at ~18:41:30 UT. The flux increase is largest for the lowest energy channels. Prior to the injection, at ~18:39:30 UT, we observe a flux intensity decrease which is most pronounced for the high energy channels. There is a first maximum, simultaneous an all energy channels, at ~ 18:43:30 UT.

The electron pitch angle distribution in Fig. 7 appears close to isotropic prior to the large flux increase associated with the electron injection. At 18:41:30 UT we observe a transition from the near isotropic distribution to a transverse distribution with a maximum around ~90° pitch angles.

3.3.3   Ions

For ions with the highest energies (>219 keV) in Fig. 3, the initial increasing trend appears as dispersive. For the highest energy channel the flux increase starts at ~18:37:30 UT, while for the two lower energy channels, it starts one and 2 min later at ~18:38:30 UT and ~18:39:30 UT, respectively. For the four intermediate energy channels (73–219 keV) there is no indication of a dispersive ion injection. For the lowest energies (<73 keV) there is a flux intensity decay starting at 18:39:30 UT. The first maxima for

energies >96 keV appear to be attained simultaneously at ~18:41:30 UT.

For the lowest ion energy interval (27.5–59 keV) in Fig. 7, the pitch angle flux distribution is anisotropic with a maximum around 90°. The transverse character of the distribution is maintained during the whole time period, but with an intensity drop starting at ~18:40 UT. For the high energy range (59–402.5 keV), the ion flux intensity distribution is anisotropic. Before the injection, the flux exhibits a minimum for pitch angles around 90°, indicating a field-aligned velocity distribution. After the injection, beginning at 18:39:30 UT, the anisotropy of the distribution is reversed and attains a maximum around 90°.

In Fig. 8, top and third panels, the components F_V- and F_D represent the integrated ion flux intensity in the radial and azimuthal directions, respectively. The radial flux, F_V, is alternatively outwards and inwards. Before onset at ~18:40 UT the average flux is small and slightly earthward, while later the amplitudes are larger with a negative average value, indicating an overall inward ion transport. The average of the azimuthal flux component, F_D, is during the whole period negative, indicating an overall westward ion transport.

3.3.4   SCATHA particle flux intensities

In Fig. 4 we show for SCATHA the differential fluxes for electrons and ions in the same pitch angle range as for GEOS-2; i.e. 65°–115°. The SCATHA flux data in Fig. 4 covers a smaller energy range than for GEOS-2; four energy channels for electrons from 19.4 keV to 140 keV and four energy channels for ions from 15.6 keV to 133 keV. The respective mean energies for the different channels are indicated on the curves.

3.3.5   Electrons

From Fig. 4, the start of the injection associated with the electron flux intensity increase on SCATHA can be localized to ~18:42:30 UT for the three highest energy channels. For the lowest energy channel (19.4 keV), the increase appears to start 1 min earlier at ~18:41:30 UT. About 2–3 min before the electron injection, at ~18:40:30 UT and ~18:39:30 UT, respectively, there is, as on GEOS-2, a flux intensity decrease on all channels. The first electron flux intensity maximum occurs simultaneously on all channels at ~ 18:44:30 UT.

3.3.6   Ions

For the two highest energy channels (133 and 71 keV) in Fig. 4, the start of the ion flux increase is somewhat uncertain, but appears to be at ~18:37:30 UT and ~18:38:30 UT, respectively. Although the timing is uncertain, the data do not contradict a dispersive injection of high energy ions. For the two lowest energy channels (15.6 keV and 36.0 keV), the fluxes have a decreasing trend.
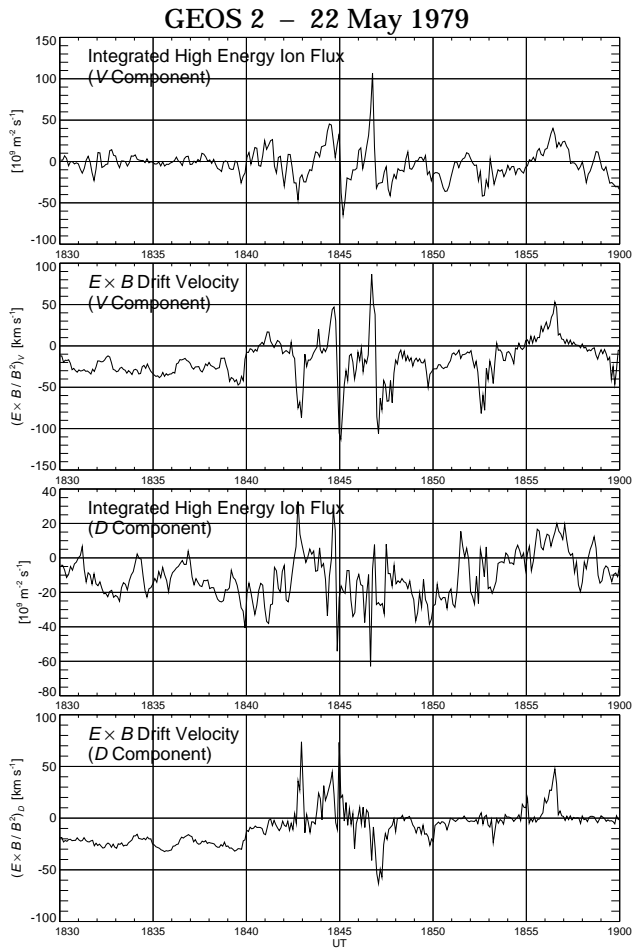
GEOS 2 – 22 May 1979

Fig. 8. GEOS-2 measurements as functions of time. From top to bottom: 1. High energy (>33 keV) radial ion flux intensity; 2. Calculated radial $E \times B$-drift velocity; 3. High energy (>33 keV) azimuthal ion flux intensity; 4. Calculated azimuthal $E \times B$–drift velocity.

3.4 High frequency oscillations

The oscillations associated with the dipolarization extend over a large frequency range from a few mHz to several Hz, and are observed on both s/c. Perraut et al. (2000) interpreted the oscillations with frequencies in the range around ∼1 Hz, the ion cyclotron frequency, as current driven Alfvén waves, and pointed out that they are consistently observed in connection with substorms. The onset of these oscillations is simultaneous with the onset of the substorm and they persist during the selected time interval.

3.4.1 GEOS-2 oscillations

In the lowest panel of Fig. 3 we have plotted the power of the magnetic fluctuations integrated between 0.5 and 11 Hz for the B-components on GEOS-2. The power is approximately constant until 18:40:40 UT when a fast growth starts. These oscillations exhibit several successive maxima; around
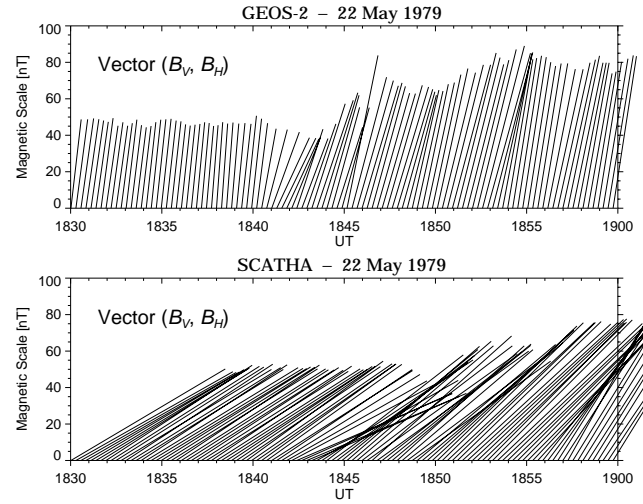

Fig. 9. Vector plots of the meridian plane magnetic field, B_H vs. B_V, for GEOS-2 and SCATHA as functions of time.

∼18:43 UT, ∼18:45 UT, ∼18:47 UT, and ∼18:53 UT. The average amplitude regains its pre–substorm level around ∼18:57 UT.

3.4.2 SCATHA oscillations

The bottom diagram of Fig. 4 illustrates the magnetic power variations recorded on SCATHA in the frequency interval 1.0–2.0 Hz. The onset of these oscillations occur at ∼18:41:30 UT. They persist during the selected time interval, however, with a reduced amplitude after ∼10 min at ∼18:50 UT.

4 Discussion

During the substorm growth-, onset-, and recovery phases, there are large variations in the magnetic and electric fields, electron and ion flux intensities, together with large oscillations over frequency ranges from a few mHz to several Hz. Simultaneous with these magnetospheric processes magnetic Pi2-oscillations are observed on the ground close to the s/c footprint.

4.1 The magnetic field

The variation of the magnetic field during the dipolarization can be illustrated by the vectorial magnetic fields in the meridian $V H$-plane in Fig. 9 and in the $D H$-plane in Fig. 10, for GEOS-2 and SCATHA, respectively. To emphasize the overall trend, filtered values have been used (periods >50 s retained). Before the dipolarization, the magnetic field at GEOS-2 is smaller and considerably less tailward directed than at SCATHA. This is consistent with GEOS-2 being below, but close to the CS midplane, and SCATHA is presumably close to the CS boundary.
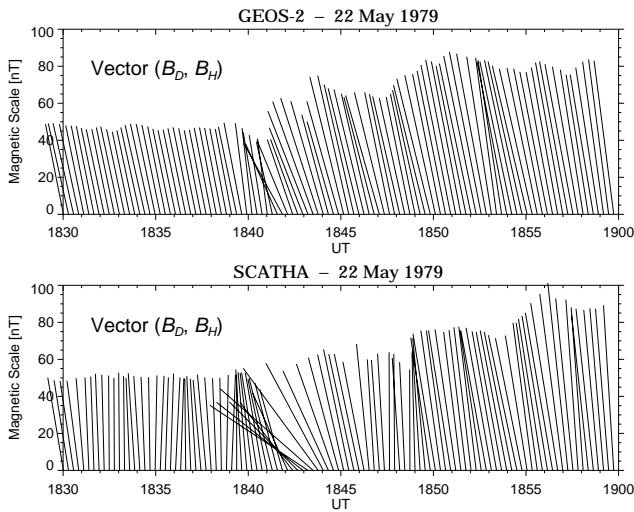
Fig. 10. Vector plots of the magnetic field normal to the meridian plane, B_H vs. B_D, for GEOS-2 and SCATHA as functions of time.

4.1.1 Westward expansion

The local commencement of the substorm and the subsequent magnetic field dipolarization is observed as directional changes of the meridian magnetic fields on GEOS-2 and SCATHA in Fig. 9. The initial indications of a developing substorm on the respective B_H-components is first seen on GEOS-2 at ~18:39:45 UT, and about 40 s later on SCATHA at ~18:40:25 UT. The delay indicates an azimuthal westward expansion of the substorm, since an inward radial expansion would first be expected at SCATHA, whose field lines intersect the MES farthest from the Earth. The delay observed on SCATHA is also apparent on the other recorded quantities: The ion injection, the initial electron flux decrease, and the electron injection are all delayed by 1 min, which is the resolution for the measurements of these quantities. For the quantities with higher resolution we estimate the delay between GEOS-2 and SCATHA to be: ~40 s for the initial B-field stretching, ~50 s for the onset of high frequency oscillations, and ~40 s for the dipolarization onset. Further, a westward expansion is not contradicted by the Sodankylä ground observations presented in Fig. 5 which, although the initial amplitudes are small, may indicate a substorm breakup occurring earlier than the first indications on the two s/c. Together with the observed ion flux dispersion, this suggests that the substorm break-up was initiated at a position to the east of the two s/c, and that the subsequent expansion was westward in accordance with the normal tendency established by the findings of Nagai (1991), Ohtani and Tamao (1993), and Thomsen et al. (2001). With an angular s/c separation of 5.75° at 18:40 UT, we find, with an estimated time delay of ~45 s, the azimuthal substorm expansion velocity to be ~7.7°/min, corresponding to ~94 km/s at geostationary distances and ~14 km/s in the ionosphere. Thus, with a breakup in the local time sector 23:00–24:00 LT, the substorm would, with a

constant expansion velocity, arrive at the GEOS-2/SCATHA position(s) with a delay of about 4–5 min.

4.1.2 Field-Aligned Birkeland Currents (FABC)

At the MES, there is, except for a small azimuthal component, only an axial magnetic field component B_H. By definition B_V is zero. The magnetospheric currents can be divided into currents normal to the magnetic field and Field Aligned Birkeland Currents (FABC). The azimuthal current component at the MES generates magnetic field components B_V and B_H in the meridian plane which at the two s/c are observed as a tailward stretching of the magnetic field during the substorm growth phase. In situations where FABCs are present, the current-magnetic field relationship is rather complicated. For symmetry reasons, the FABCs vanish at the MES, but off the MES, however, FABCs can generate magnetic fields with all components present. In particular, ΔB_D changes in the B_D-component off the MES, are interpreted as a signature of FABCs, e.g. Coleman et al. (1976), McPherron and Barfield (1980), and Kokobun and McPherron (1981). Weak FABCs before the substorm onset flow mainly in the meridian plane, but as the substorm develops, and the FABCs become strong, they are tilted in the azimuthal direction along with the magnetic field. The magnetic field azimuthal tilt, which is seen in Fig. 10 between ~18:41 UT and ~18:46 UT, is, as expected from the s/c positions relative to the MES, most pronounced on SCATHA.

4.1.3 Magnetic field variations

For the discussion of the magnetic field variations, we qualitatively separate the substorm time sequence into four periods which are closely related to the behaviour of the azimuthal B_D-component on SCATHA.

4.1.4 B_D small and positive

According to Fig. 3, the variations of the GEOS-2 magnetic field components are quite small before the substorm onset. On SCATHA, Fig. 4, however, small but recognizable variations can be identified prior to ~18:40 UT on all three components. In particular, there is an increase in the B_D-component from a negative value to a value close to zero. For undisturbed conditions at geostationary distances, the azimuthal B_D-component normally exhibits a small negative offset (a few nT). Thus, before dipolarization onset, while the s/c is located to the west of the DPR, the increase in B_D indicates the presence of FABCs. The modest magnetic field changes on SCATHA, $\Delta B_D > 0$, $\Delta B_V < 0$, and $\Delta B_H > 0$, are consistent with weak downward FABCs, both tail- and eastward of the s/c.

4.1.5 B_D negative and decreasing

Starting at ~18:39:00 UT the SCATHA azimuthal B_D-component becomes negative followed by a large (negative) increase, $\Delta B_D \sim$-50 nT. A negative B_D change

can be generated either by an upgoing current tailward, or a downgoing current earthward of the s/c. The B_D-component thus added to the (meridian) magnetic field results in an azimuthally tilted magnetic field, as seen in Fig. 10, which below the MES conducts azimuthally tilted FABCs. These currents in turn, generate meridian plane magnetic field components. On SCATHA, beginning at ∼18:40:25 UT, we observe a decreasing axial B_H-component ($\Delta B_H \sim$ -20 nT), and, beginning at 18:41:20 UT, an increasing radial B_V-component ($\Delta B_V \sim$ 15 nT). These changes represent an additional tailward stretching of the magnetic field, and are consistent with the initial 2-min directional magnetic field change beginning at ∼18:39:45 UT on GEOS-2 and at ∼18:40:25 UT on SCATHA, as seen in Fig. 9. This kind of tailward magnetic field stretching is a common feature at substorm onset (Kokobun and McPherron, 1981; Nagai, 1982, 1987; Nagai et al., 1987). With the s/c to the west of the approaching substorm, we interpret the observed tailward stretching of the magnetic field ($\Delta B_V > 0$; $\Delta B_H < 0$) on SCATHA as the result of a westward tilted upgoing FABC tailward of the s/c.

4.1.6 B_D negative and increasing

The transition towards a more dipolar-like structure (Fig. 9) begins at ∼18:42:30 UT on GEOS-2 and at ∼18:43:10 UT on SCATHA. The beginning of the dipolar recovery coincides with the minimum values of the axial B_H-components on both s/c as observed on Fig. 3 and Fig. 4 for GEOS-2 and SCATHA, respectively. At SCATHA it closely coincides with both the large maximum magnitude of the negative azimuthal component B_D at 18:43:10 UT, and the maximum of the B_V-component at 1842:45 UT (Fig. 4). The subsequent relative variations of the SCATHA magnetic components are: $\Delta B_V < 0$, $\Delta B_D > 0$, and $\Delta B_H > 0$, which are consistent with an azimuthally receeding upgoing FABC tail- and westward of SCATHA. As seen in Fig. 3, the changes in the magnetic field components are qualitatively similar on GEOS-2, but, except for B_H, less pronounced. The weaker response to the FABCs is consistent with the position of GEOS-2 being close to the MES.

The variations of the magnetic field components suggest that the strong upgoing FABC region moved past SCATHA from east to west on the tailward side. Further, the observed maxima/minima indicate that the central part of the FABC system passed SCATHA at ∼18:43:10 UT and about 45 s earlier for GEOS-2.

4.1.7 B_D small and positive

After the passage of the strong FABC region, the effect of the FABCs diminish, as clearly observed from the SCATHA B_D-component in Fig. 4, which at ∼18:46 UT attains its initial value centered around −10 nT. There is, however, a further decrease in its magnitude to a B_D-value around zero, as observed during the pre–substorm growth period, indicating a possible weak downward FABC tailward of SCATHA for

a 4-min period from ∼18:46 to ∼18:50 UT. The magnetic fields on both s/c approach a dipolar structure, indicating a partially disrupted azimuthal current in the vicinity of the s/c. On SCATHA the final transition towards dipolarization begins at ∼18:55 UT.

A partially disrupted westward azimuthal current can be regarded as the result of a superimposed equivalent eastward current. Below the MES and earthward of this current, the result would be variations $\Delta B_H > 0$ and $\Delta B_V < 0$, while at the MES, $\Delta B_V \sim B_V \sim 0$. On GEOS-2, a small but long lasting positive shift $\Delta B_V \sim 10$ nT at 18:41 UT is observed, indicating a northward shift of the MES, and thus bringing the relative position of GEOS-2 somewhat below the MES.

The upward FABCs clearly attain a maximum and then diminish while the (increasing) equivalent eastward azimuthal current, representing the disrupted part of the original current, gradually becomes dominant. The main part of the upward FABCs lasts for ∼3–4 min, and with the estimated azimuthal expansion velocity of ∼7.7°/min may cover an azimuthal range of ∼22–31°. As already pointed out, the SCATHA B_D-component (Fig. 4) indicates weaker downgoing field-aligned current structures both before and after the arrival of the upward FABC structure.

4.2 Particle injections

Before the onset of the local dipolarization, the current which maintains the tailward structure is, on the microscopic scale, carried by azimuthally gradient- and curvature-drifting particles. The electrons drifting towards the s/c from the west, are not accelerated prior to the encounter with the DPR, while the ions drifting towards the s/c from the east have traversed the boundary of the DPR.

When the DPR encounter the s/c, the observed electrons (at all energies) are passing from a region of weak tailward magnetic field to a region with stronger dipolar-like field. The expected dispersionless electron flux intensity increase, or electron injection, is confirmed by the differential flux intensities presented in the second panels in Figs. 3 and 4 for GEOS-2 and SCATHA, respectively. The estimated electron injection at ∼18:41:30 UT on GEOS-2 and at ∼18:42:30 UT on SCATHA, represents a delay of ∼1 min, which is comparable to the time resolution of the measurements.

About 2 min before the electron injection, the flux intensities decrease by almost an order of magnitude for some energy channels on both s/c.

Although the time resolution does not allow a precise timing, these electron "ejections" apparently coincide with the tailward stretching of the magnetic field observed on both s/c about 2 min prior to the start of the dipolarization.

Compared with the electrons, the situation is quite different for the westward drifting ions. The ion gradient- and curvature-drifts in the dipolarized magnetic field are in the same direction as the westward expansion of the DPR. The first indication of injected ions at GEOS-2 is at ∼18:37:30 UT for the highest energy channel (Fig. 3), while on SCATHA, at a lower energy, it is at ∼18:38:30 UT

Table 2. Timing of parameter changes at SCATHA and GEOS-2.

	GEOS-2 ~UT	SCATHA ~UT
High energy ions[1]	18:37:30	18:38:30
Start upward FABC		18:39:00
B-field stretching	18:39:45	18:40:25
Electron flux decrease[1]	18:39:30	18:40:30
HF-waves	18:40:40	18:41:30
Strong increase in FABC		18:41:40
Electron injection[1]	18:41:30	18:42:30
Dipolarization start	18:42:30	18:43:10
Max upward FABC		18:43:10

[1] 1 min resolution

(Fig. 4). On both s/c there appears to be a dispersion for the highest energy ions which are injected about 4-5 min before the injection of the electrons. It is not possible to identify the time delay between the two s/c from the energy dependent dispersive ion injections.

4.3 Event sequence

Even with a somewhat uncertain timing of the different processes observed, we may qualitatively and to some extent quantitatively, identify the sequence of events preceeding the substorm dipolarization.

At the position of the two s/c, the first indication of an approaching substorm is the arrival of dispersive high energy ions, with the highest energy arriving at GEOS-2 at ~18:37:30 UT and at SCATHA about 1 min later. Then, on SCATHA at ~18:39 UT we deduce from the recorded B_D component a change to an upward directed FABC. At ~18:39:45 UT on GEOS-2 and about 40 s later, at ~18:40:25 UT on SCATHA, we observe a tailward stretching of the meridian magnetic field, whith a simultaneous electron flux decrease on the two s/c. About one min later, we identify on both s/c the onset of high frequency waves; at 18:40:40 UT on GEOS-2 (0.5–11 Hz) and at 18:41:30 UT on SCATHA (1.0–2.0 Hz). Simultaneous with these waves we note, on basis of the SCATHA B_D–component, a rapid increase in the upward FABC, beginning at ~18:41:40 UT. At ~18:41:30 UT and at ~18:42:30 UT on GEOS-2 and SCATHA, respectively, a strong increase in the electron flux, i.e. electron injection, is observed. The electron injection starts about 1 min prior to the dipolarization onset, which appears on GEOS-2 at ~18:42:30 UT and on SCATHA at ~18:43:10 UT. When the dipolarization starts on SCATHA, we observe a simultaneous minimum of B_D, corresponding to a maximum upward FABC. The event sequence is summarized in Table 2.

4.4 Ballooning instability

There has been a number of suggestions related to the mechanisms which are at the origin of substorm onset and development. The drift ballooning instability, originally suggested by Roux (1985) and Roux et al. (1991), has clearly been the major candidate to explain the onset and development of substorms (e.g. Ohtani et al., 1989a,b; Miura et al., 1989; Ohtani and Tamao, 1993; Lee and Wolf, 1992; Lee, 1998; Hurricane et al., 1997; Cheng and Lui, 1998; Bhattacharjee et al., 1998a,b; Horton et al., 1999; Hurricane et al., 1999; Horton et al., 2001).

The ballooning instability mechanism associated with a substorm is qualitatively similar to the Rayleigh–Taylor instability. With ion and electron diamagnetic drifts in opposite directions and normal to the respective pressure gradients and the magnetic field **B**, the resulting electron and ion diamagnetic currents flow along the respective constant pressure surfaces. Prior to substorm onset, during the growth phase, the current sheet is in quasi–equilibrium with the azimuthal diamagnetic current with **j** being related to the pressure gradient ∇p by $\mathbf{j} = \mathbf{B} \times \nabla p / B^2$.

With density perturbations of the equilibrium the opposite directions of the electron and ion fluxes tend to create space charges. The associated electric fields **E**, combined with the ambient magnetic field **B**, result in additional drifts, $\mathbf{v}_E = \mathbf{E} \times \mathbf{B} / B^2$, which amplify the perturbation. To maintain quasi–neutrality, any tendency to accumulate space charges is, however, counteracted by neutralizing currents along the magnetic field lines. If these FABCs constitute part of closed current circuits (via the ionosphere), they will tend to neutralize the electric fields and thus inhibit the growth of an instability.

Although GEOS-2 and SCATHA are well outside the region of substorm onset, signatures which are associated with ballooning instabilities are observed. These signatures may be of relevance for an understanding of the substorm expansion mechanism.

4.4.1 Birkeland currents

The FABCs necessary to maintain quasi-neutrality produce additional magnetic field components. From symmetry reasons, these components, as the FABCs, vanish at the MES and increase away from the MES. FABCs in the meridian plane will produce azimuthal magnetic field components, earth- and tailward of the currents, which, in turn modify the direction of the FABCs, which, away from the MES, attain significant azimuthal components.

The difference in the azimuthal magnetic components recorded on the two s/c is evident from Figs. 3 and 4 for GEOS-2 and SCATHA, respectively. Clearly SCATHA, which is farthest away from the MES, records the largest values in accordance with what is expected for azimuthal magnetic field components produced by symmetric FABCs. The temporary, strong B_D-component at SCATHA implies that below the MES the magnetic field, in addition to the tailward

direction, is strongly tilted azimuthally across the meridian plane. A FABC will also generate magnetic field components in the V- and H-directions. The recorded changes, $\Delta B_V < 0$ and $\Delta B_H > 0$, are consistent with the s/c being earthward and initially westward of the FABCs.

4.4.2 $E \times B$ dominated radial particle flux

The ballooning instability is associated with ion fluxes in the radial direction composed of both $E \times B$-drifts due to the E_D-component, and diamagnetic drifts caused by the azimuthal pressure gradient of the perturbation. These ion drifts are 90° out of phase. Hence, if one of the drifts dominates, the measured ion flux oscillations would be either in phase or 90° out of phase with the $E \times B$-drift. In Fig. 8 we present four panels related to the particle fluxes recorded on GEOS-2. The first and the third panel from the top represent the integrated ion flux intensity in the radial and azimuthal directions for energies >33 keV, respectively, while the second and the fourth panel represent the $E \times B$-drifts in the corresponding directions. Prior to the substorm onset (at ~18:40 UT) the GEOS-2 electric field cannot be used with confidence because of a satellite current that is too small.

A comparison of the radial ion flux intensity (Fig. 8, top panel) with the radial $E \times B$-drift (Fig. 8, second panel), shows a distinct in phase correlation for the period after 18:40 UT. Thus, the azimuthal electric field, with the associated $E \times B$-drift, dominates the radial particle transport and hence the development of the substorm, as discussed in detail by Le Contel (2001) for two other events recorded on GEOS-2. The observed correlation of the $E \times B$-drift and the radial ion flux intensity represents supporting evidence for the presence of ballooning modes during the azimuhal expansion of the substorm.

A similar comparison for the azimuthal ion flux intensity (Fig. 8, third panel) and $E \times B$-drift (Fig. 8, bottom panel), does not reveal similar correlations as for the radial direction. We note, however, the westward azimuthal ion flux, related to the ion curvature and gradient drifts.

5   Summary

A substorm on 22 May 1979 was simultaneously observed on the geosynchronous satellite GEOS-2 and SCATHA when they were separated by less than 30 min in local time, close to 21:00 LT, with SCATHA somewhat earthward of GEOS-2. GEOS-2 was close to the current sheet midplane at the magnetic equatorial surface, while SCATHA was close to the current sheet southward boundary. The first indication of an approaching substorm was the injection of dispersed high energy ions, consistent with high energy ions drifting westward, with a velocity above the substorm expansion velocity. The first indication on the magnetic field was recorded about 2 min later as an initial tailward magnetic field stretching, which coincided with a decay of the measured flux intensity of ~ 90° pitch angle electrons. Apparently, large pitch

angle electrons are first "ejected" before being injected when the magnetic field begins the recovery of a more dipolar-like structure. These substorm onset indications were first recorded on GEOS-2. The estimated delay of 45 to 60 s between the GEOS-2 and SCATHA recordings was consistent with a westward expansion of the substorm boundary, with a velocity of about ~7.7°/min. Following the substorm onset, the most apparent difference in the recordings at the two s/c, was the significantly larger magnitude of the azimuthal magnetic field component recorded on SCATHA. The strong B_D-component at SCATHA lasted about 3 min and was, together with the variations of the other components B_V and B_H, consistent with a strong upward field-aligned Birkeland current structure below the magnetic equatorial surface. The current structure was moving past the s/c on the tailward side from east to west.

Both before and after the passage of the current structure, the azimuthal B_D-component on SCATHA indicates weak downward field-aligned currents.

As the large amount of cited papers suggest, the ballooning instability is, as suggested by Roux (1985) and Roux et al. (1991), a major candidate for understanding the substorm onset and development. A simple qualitative (Rayleigh–Taylor) instability model at the magnetic equator suggests possible ballooning instability signatures. The strong temporary azimuthal magnetic field component recorded well below the magnetic equatorial plane at SCATHA, represents a clear signature of strong substorm associated field-aligned currents; the measured radial high energy ion flux is highly correlated with the instability generated $E \times B$-drift during the substorm.

References

Akasofu, S.-I.: The development of the auroral substorm, Planet. Space Sci., 12, 273, 1964.

Bhattacharjee, A., Ma, Z. W., and Wang, X.: Ballooning instability of a thin current sheet in the high–Lundquist–number magnetotail, Geophys. Res. Lett. 25, 861–864, 1998a.

Bhattacharjee, A., Ma, Z. W., and Wang, X.: Dynamics of thin current sheets and their disruption by ballooning instabilities: A mechanism for magnetospheric substorms, Phys. of Plasmas, 5, 2001–2009, 1998b.

Cheng, C. Z. and Lui, A. T. Y.: Kinetic ballooning instability for substorm onset and current disruption observed by AMPTE/CCE, Geophys. Res. Lett., 25, 4091–4094, 1998.

Coleman Jr., P. J. and McPherron, R. L.: Fluctuations in the distant geomagnetic field during substorms: ATS 1, in Particles and Fields in the Magnetosphere, edited by McCormac, B. M., Reidel, Mass., 171–194, 1976.

Cummings, C. D., Barfield, J. N., and Coleman Jr., P. J.: Magnetospheric substorms observed at the synchronous orbit, J. Geophys. Res., 73, 6687–6698, 1968.

Fairfield, D. H. and Ness, N. F.: Configuration of the magnetic tail during substorms, J. Geophys. Res., 75, 7032–7047, 1970.

Holter, Ø., Altman, C., Roux, A., Perraut, S., Pedersen, A., Pécseli, H., Lybekk, B., Trulsen, J., Korth, A., and Kremser, G.: Characterization of Low Frequency Oscillations at Substorm Breakup, J. Geophys. Res., 100, 19 109–19 119, 1995.

Horton, W., Wong, H. V., and Van Dam, J. W.: Substorm trigger condition, J. Geophys. Res., 104, 22 745–22 757, 1999.

Horton, W., Wong, H. V., Van Dam, J. W., and Crabtree, C.: Stability properies of high-pressure geotail flux tubes, J. Geophys. Res., 106, 18 803–18 822, 2001.

Hurricane, O. A., Fong, B. H., and Cowley, S. C.: Nonlinear magnetohydodynamic detonation: Part I, Phys. Plasmas, 4, 3565–3580, 1997.

Hurricane, O. A., Fong, B. H., Cowley, S. C., Coroniti, F. V., Kennel, C. F., and Pellat, R.: Substorm detonation, J. Geophys. Res., 104, 10 221–10 231, 1999.

Jacquey, C., Sauvaud, J. A., and Dandouras, J.: Location and propagation of the magnetotail current disruption during substorm expansion: Analysis and simulation of an ISSE multi-onset event, J. Geophys. Res. Lett., 18, 389–392, 1991.

Jacquey, C., Sauvaud, J. A., Dandouras, J., and Korth, A.: Tailward propagating cross-tail current disruption and dynamics of near-Earth tail: A multipoint measurement analysis, J. Geophys. Res. Letts., 20, 983–986, 1993.

Kokobun, S. and McPherron, R. L.: Substorm signatures at synchronous altitude, J. Geophys. Res., 86, 11 265–11 277, 1981.

Lee, D. Y.: Ballooning instability in the tail plasma sheet, Geophys. Res. Lett., 25, 4095–4098, 1998.

Lee, D. Y. and Wolf, R. A.: Is the Earth's magnetotail balloon unstable?, J. Geophys. Res., 97, 19 251–19 257, 1992.

Le Contel, O., Roux, A., Perraut, S., Pellat, R., Holter, Ø., Pedersen, A., and Korth, A.: Possible control of plasma transport in the near–Earth plasma sheet via current driven Alfvén waves ($f \simeq F_{H+}$), J. Geophys. Res., 106, 10 817–10 827, 2001.

McPherron, R. L.: Substorm related changes in the geomagnetic tail: The growth phase, Planet. Space Sci., 20, 1521–1539, 1972.

McPherron, R. L., Russel, C. T., and Aubry, M. P.: Satellite Studies of Magnetospheric Substorms on 15 August 1968, 9. Phenomenological Model of Substorms, J. Geophys. Res., 78, 3131–3149, 1973.

McPherron, R. L. and Barfield, J. N.: A seasonal change in the effect of field-aligned currents at synchronous orbit, J. Geophys. Res., 85, 6743–6746, 1980.

Miura, A., Ohtani, S., and Tamao, T.: Balloning Instability and Structure of Diamagnetic Hydromagnetic Waves in a Model Magnetosphere, J. Geophys. Res., 94, 15 231–15 242, 1989.

Nagai, T.: Observed magnetic substorms signatures at synchronous altitudes, J. Geophys. Res., 87, 4405–4417, 1982.

Nagai, T.: Field-Aligned Currents Associated with Substorms in the Vicinity of Synchronous Orbit, 2. GOES 2 and GOES 3 Observations, J. Geophys. Res., 92, 2432–2446, 1987.

Nagai, T.: An Empirical Model of Substorm-Related Magnetic Field Variations at Synchronous Orbit, Magnetospheric Substorms, in Geophys. Monogr., edited by Kan, J. R. , Potemra, T. A., Kokobun, S., and Iijima, T., 64, 91–95, AGU, Washington D.C., 1991.

Nagai,T., Singer, H. J., Ledley, B. G., and Olsen, R. C.: Field-aligned currents associated with substorms in the vicinity of synchronous orbit, 1. The 5 July 1979 substorm observed by SCATHA, GOES 3, and GOES 2, J. Geophys.Res., 92, 2445–2431, 1987.

Ohtani, S.: Earthward expansion of tail current disruption: Dual-satellite study, J. Geophys. Res., 103, 6815–6825, 1998.

Ohtani, S., Kokobun, S., and Russel, C. T.: Radial expansion of the tail current disruption during substorms: A new approach to the substorm onset region, J. Geophys. Res., 97, 3129–3136, 1992.

Ohtani, S., Miura, A., and Tamao, T.: Coupling between Alfvén and slow magnetosonic waves in an inhomogeneous finite-β plasma, I. Coupled equations and and physical mechanism, Planet. Space Sci., 37, 567–577, 1989a.

Ohtani, S., Miura, A., and Tamao, T.: Coupling between Alfvén and slow magnetosonic waves in an inhomogeneous finite-β plasma, II. Eigenmode analysis of localized ballooning-interchange instability, Planet. Space Sci., 37, 579–588, 1989b.

Ohtani, S., Takahashi, K., Higuchi, A., Lui, A. T. Y., Spence, H., and Fennel, J. F.: AMPTE/CCE-SCATHA simultaneous observations of substorm-associated magnetic fluctuations, J. Geophys. Res., 103, 4671–4682, 1998.

Ohtani, S., Takahashi, K., Zanetti, L. J., Potemra, T. A., McEntire, R. W., and Ijima, T.: Tail current disruption in the geosynchronous region, Magnetospheric Substorms, in Geophys. Monogr., edited by Kan, J. R. , Potemra, T. A., Kokobun, S., and Iijima, T., 64, AGU, Washington D.C., 131–137, 1991.

Ohtani, S. and Tamao, T.: Does the Ballooning Instability Trigger Substorms in the Near-Earth Magnetotail?, J. Geophys. Res., 98, 19 369–19 379, 1993.

Perraut, S., Le Contel, O., Roux, A., Pellat, R., Korth, A., Holter, Ø., and Pedersen, A.: Disruption of parallel current at substorm breakup, J. Geophys. Res. Letts., 27, 4041–4044, 2000.

Roux, A., Perraut, S., Robert, P., Morane, A., Pedersen, A., Korth, A., Kremser, G., Aparicio, B., Rogers, D., and Pellinen, R.: Plasma Sheet Instability Related to the Westward Traveling Surge, J. Geophys.Res., 96, 17 697–17 714, 1991.

Roux, A.: Generation of field-aligned current structures at substorm onsets, in Proceedings ESA Workshop on Future Missions in Solar, Heliospheric, and Space Plasma Physics, Garmisch-Partenkirchen, ESA SP–235, 151, 1985.

Thomsen, M. F., Birn, J., Borovsky, J. E., Morzinski, K., McComas, D. J., and Reeves, G. D.: Two-satellite observations of substorm injections at geosynchronous orbit, J. Geophys. Res., 106, 8405–8416, 2001.